Published in final edited form as:
Ann Biomed Eng. 2011 February ; 39(2): 897–910. doi:10.1007/s10439-010-0184-2.

Numerical Investigation of the Effects of Channel Geometry on Platelet Activation and Blood Damage

Jingshu Wu[1], **B. Min Yun**[1], **Anna M. Fallon**[2], **Stephen R. Hanson**[3], **Cyrus K. Aidun**[1], and **Ajit P. Yoganathan**[2,4]

[1]G. W. Woodruff School of Mechanical Engineering, Georgia Institute of Technology, Atlanta, GA, USA

[2]School of Chemical and Biomolecular Engineering, Georgia Institute of Technology, Atlanta, GA, USA

[3]Department of Biomedical Engineering, Oregon Graduate Institute, Beaverton, OR, USA

[4]Wallace H. Coulter Department of Biomedical Engineering, Georgia Institute of Technology & Emory University, 313 Ferst Drive, Whitaker Building, Room 2119, Atlanta, GA 30332-0535, USA

Abstract

Thromboembolic complications in Bileaflet mechanical heart valves (BMHVs) are believed to be due to the combination of high shear stresses and large recirculation regions. Relating blood damage to design geometry is therefore essential to ultimately optimize the design of BMHVs. The aim of this research is to quantitatively study the effect of 3D channel geometry on shear-induced platelet activation and aggregation, and to choose an appropriate blood damage index (BDI) model for future numerical simulations. The simulations in this study use a recently developed lattice-Boltzmann with external boundary force (LBM-EBF) method [Wu, J., and C. K. Aidun. *Int. J. Numer. Method Fluids* 62(7):765–783, 2010; Wu, J., and C. K. Aidun. *Int. J. Multiphase flow* 36:202–209, 2010]. The channel geometries and flow conditions are re-constructed from recent experiments by Fallon [The Development of a Novel in vitro Flow System to Evaluate Platelet Activation and Procoagulant Potential Induced by Bileaflet Mechanical Heart Valve Leakage Jets in School of Chemical and Biomolecular Engineering. Atlanta: Georgia Institute of Technology] and Fallon *et al*. [*Ann. Biomed. Eng*. 36(1):1]. The fluid flow is computed on a fixed regular ‘lattice’ using the LBM, and each platelet is mapped onto a Lagrangian frame moving continuously throughout the fluid domain. The two-way fluid–solid interactions are determined by the EBF method by enforcing a no-slip condition on the platelet surface. The motion and orientation of the platelet are obtained from Newtonian dynamics equations. The numerical results show that sharp corners or sudden shape transitions will increase blood damage. Fallon’s experimental results were used as a basis for choosing the appropriate BDI model for use in future computational simulations of flow through BMHVs.

Keywords

Fluid mechanics; Blood damage index; CFD; Platelet activation; Channel flow; Optimization

Address correspondence to Ajit P. Yoganathan, Wallace H. Coulter Department of Biomedical Engineering, Georgia Institute of Technology & Emory University, 313 Ferst Drive, Whitaker Building, Room 2119, Atlanta, GA 30332-0535, USA. ajit.yoganathan@bme.gatech.edu.

INTRODUCTION

Bileaflet mechanical heart valves (BMHVs) have been widely used to replace defective native heart valves. Unfortunately, the design of BMHVs produces flow fields that may cause damage to blood elements, especially in the hinge area. Initial experimental work by Fallon *et al.*[8,9] proved that channel geometry has a strong impact on platelet activation. In later studies,[6,7] Fallon measured the Thrombin-Antithrombin III (TAT) concentration of blood flow through channels with different geometries and constriction diameter sizes. She concluded that for channels with smaller constriction diameter, size is more important to TAT formation than the geometry. However, for the larger constriction diameter channels, the geometry plays an important role. High fidelity simulations of the valve flow fields throughout the cardiac cycle are required to improve and refine existing valve designs in order to ultimately develop BMHVs with minimal thromboembolic complications.

The objectives of this study are to analyze the flow properties for different channel geometries, and to choose an appropriate blood damage index (BDI) model by matching Fallon's experimental results. The new lattice-Boltzmann method with external boundary force (LBM-EBF) computational method can help researchers further understand the cause of blood damage, and improve BMHV design to reduce the adverse hemodynamic effects of valves that cause platelet activation and blood element damage. The LBM is an accurate and efficient fluid solver that provides several advantages over other Navier–Stokes flow solvers. The EBF method is used for fluid–solid coupling and is used for the modeling of suspended particles.

It has been established in previous studies[29,30] that hemodynamic shear stress is a primary biomechanical trigger for thromboembolic events. It is also well known that exposure time to shear stress is a critical parameter for platelet activation.[5,10,16,20,22] Several BDI models have been presented and used in previous studies as a measure of blood damage. Bluestein *et al.*[3,5,20] define the platelet activation state (PAS) to model blood damage under unsteady flow conditions. Grigioni *et al.*[11] developed a mathematical model to evaluate red blood cell damage. Based on this model, Nobili *et al.*[20] calculated platelet activation and compared their simulation results with experimental data. In this model, a non-linear least-square fitting method was applied to obtain the model parameters. The platelet shear stress history in the previous cycle was also counted in the PAS model by a damage accumulation model.

Dumont *et al.*[5] applied a similar model without the damage accumulation to compare the hemodynamic performance of two BMHVs. With a linear shear stress–exposure time model, the cumulative effects of shear stress and exposure time on a platelet can be computed as

$$\mathrm{BDI}_{\mathrm{D}} = \frac{1}{n}\sum_{i=0}^{n} \tau_i \cdot \Delta t_i, \tag{1}$$

where $\mathrm{BDI}_{\mathrm{D}}$ is the BDI, τ_i the principal surface shear stress, and Δt_i the exposure time of platelet i.

Other studies, however, have shown that the shear stress threshold for platelet activation is independent of exposure time.[13] Tambasco and Steinman[22] included a threshold shear stress parameter in the linear BDI model that only considers platelets that have experienced high shear stress above a threshold level. Tambasco and Steinman's BDI model is defined as

$$\mathrm{BDI}_T = \frac{1}{n}\sum_{i=0}^{n} \tau_i^* \cdot \Delta t_i^*, \tag{2}$$

where BDI_T is the BDI, τ_i* the principal shear stress above the threshold, and Δt_i* the exposure time. Tambasco and Steinman estimated the threshold shear stress for platelet activation to be 105 dyn/cm^2. The same threshold value was used in this study.

In the two aforementioned models (Eqs. 1 and 2), the relationship between surface shear stress, exposure time, and BDI is linear. Other researchers found the actual relationship to be more complex. Wurzinger *et al*.[28–30] have found a non-linear relationship between blood damage, shear stress, and exposure time by measuring the amount of cytoplasm enzyme (LDH) released by platelets (which is proportional to the level of platelet activation) using a Couette-viscometer. The Couette-viscometer was used to maintain the shear rate while the LDH was measured by taking samples at a fixed time interval.

Based on these observations, a mathematical correlation to calculate the blood damage level was developed by Giersiepen *et al*.[10] It was argued that the platelet shear stress was more important than the exposure time, so high shear stress should dominate the result of the BDI equation. Giersiepen *et al*. derived a model for the BDI from the experimental results, given by

$$\mathrm{BDI}_G = \frac{1}{n}\sum_{i=0}^{n} \tau_i^{3.075} \cdot \Delta t_i^{0.77}. \tag{3}$$

This study will use Fallon's experimental results[6,7,9] as a basis for determining the appropriate numerical methodology for investigating the blood damage of platelets in BMHV hinge flow. To accomplish this task, we evaluate and compare the three different BDI models described above. In this study, we use a recently developed numerical method[26] to simulate flow with a large number of platelets. We calculate the BDI value for flow through each of the different geometries used in the experiments by Fallon. By comparing the simulation results with the existing experimental results,[6,7] we can evaluate the viability of each of the BDI models to establish a correlation between shear stress on the platelets and the level of blood damage, and to further validate our computational method for analysis of blood damage through the hinge area of BMHVs.

METHODS

Experimental Setup

In Fallon's experiments,[6,7] four different channel geometries were studied with small (400 μm) and large (800 μm) minimum diameters as shown in Fig. 1. The aim of the study was to assess the procoagulant properties of stenotic and expansive orifices designed to model the hinge regions of BMHVs that are presently in use or that have been developed in the past. Specifically, the channel geometries are similar to the contraction area and transition geometry of the hinge regions of the St. Jude Medical and Medtronic Parallel BMHVs. These different orifices were designed to represent different nuances that could be present in hinge geometries and were placed in an *in vitro* steady flow loop designed to approximate the leakage phase of the cardiac cycle.

Whole human blood was drawn for use in the experiments with the addition of 3.2% sodium citrate at a 10:1 blood to citrate ratio. Platelet counts averaged 170,000 ± 65,000 cells/μL.

The total volume of the flow loop was approximately 77 mL. The channels were placed in a chamber and the pressure upstream of the orifices was maintained by a Biomedicus (Biomedicus TX50, Minneapolis, MN, USA) centrifugal bypass pump at 120 mmHg (±5 mmHg). The flow rate was also monitored during the experiment with an inline flow meter and flow transducer supplied with the Biomedicus centrifugal pump, and the fluctuation of the flow rate was less than 0.1 L/min.

Two 0.5 mL samples were taken at 0, 15, 30, 45, and 60 min for TAT, PF4, and hemolysis assays. These samples were placed in 3 mL EDTA Vacutainer tubes for TAT and hemolysis assays and in a mixture of aspirin, acid citrate dextrose, and Prostaglandin E1 for the PF4 assay. This volume was replaced with 1 mL of saline after each sample was withdrawn. The samples were centrifuged at 14,000 RPM for 15 min at room temperature to obtain platelet poor plasma. The plasma was frozen at 4 °C until it was assayed for TAT, PF4, and hemoglobin concentrations. Details of the three assay methodologies are given in the Appendix.

Statistics were performed using non-parametric methods to compare experimental results for the different channel geometries. Each experimental group had an n-value of 6 based on a power analysis with a p-value <0.05 showing statistical significance between the groups. The Kruskal Wallace test was used to initially determine the influential variables that affected the end quantitative measures, and the Mann–Whitney test was used to show statistical significance between the groups.

Extensive details of the experimental work and methodology can be found in the works by Fallon *et al*.[6,7]

BDI Calculation

To match the numerical simulations with the experimental results, the same eight channel geometries used in the experimental setup were simulated in the computational model. The LBM-EBF, described in the following section, is used to numerically simulate platelet flow through the same eight channel geometries.

The platelets are modeled as ellipsoidal particles and are assumed to be neutrally buoyant in the suspending plasma. The platelets are released evenly and simultaneously along the radius of the channel with random azimuth angles at the channel inlet. An excessive number of platelets will result in overcrowding and an extremely large channel migration time for platelets that are close to the wall. Thus, 40 platelets are chosen as optimal for the simulations to limit overcrowding. The maximum shear stress of the platelet surface and the exposure time are recorded for all of the platelets. Three different BDI values are then calculated for each platelet using the three different BDI models described above. The BDI values for each platelet are weighted with the local flow rate at its initial position. The BDI values for the platelets are then accumulated for each channel to determine the total BDI value for the channel. This accumulation method is applied for each of the eight channels and for each of the three BDI models.

A secondary approach is also used to determine the BDI values for platelet flow through the eight channels. In the secondary method, the platelets will be released uniformly at the inlet of the fluid domain as before, but an additional random disturbance force will be added to make sure that the recirculation zones are included in the platelet flow and BDI calculation. A BDI model without damage accumulation will be applied so that only the flow conditions and channel geometry affect the BDI values. The BDI value of every platelet will be weighted by the local platelet concentration at the initial position. The BDI values for the platelets will then be accumulated for each channel to determine the total BDI value for each

of the eight channels. The reasoning for this secondary method will be explained in further detail in the “Discussion” section.

After calculation of the total BDI values for each of the eight channels and each BDI model, a comparison will be made with the experimental results of Fallon *et al*.[6,7] This comparison of the experimental results of flow through the channels with the simulated BDI value results will determine the most accurate BDI model for assessing blood damage. This will be useful in future work of exploring blood damage in BMHVs.

LBM-EBF Overview

The LBM-EBF is a novel suspension flow modeling method. The LBM is a fluid flow solver and will be described in the following section. The motion and orientation of the solid particles is solved using Newtonian dynamics equations for linear and angular momentum. The interaction between the fluid and solid phases is computed using the EBF method, which will be described below. A simple flowchart demonstrating the LBM-EBF method is shown in Fig. 2.

LBM for Solving Fluid Flow

The numerical method used to solve the fluid phase is the LBM, which is a well-validated[1,2] technique for direct numerical simulations of fluid flow. In the LBM, the fluid is modeled as a continuous distribution of fictitious fluid particles that exist on a fixed regular ‘lattice’ grid that represents the 3D velocity space. Each node on this grid is linked to neighboring nodes through lattice velocity vector links. The fluid particle distribution functions are related to important macroscopic fluid properties such as density and velocity.

The fluid particle distribution changes with time through processes known as ‘streaming’ and ‘collision.’ In the ‘streaming’ process, the fluid particles move to neighboring grid nodes that are connected by lattice velocity links. In ‘collision,’ fluid particles arriving at the same node at the same time collide with each other and change the fluid particle distribution at that node. These processes dictate the time evolution of the fluid particle distribution at each grid node and only require knowledge of the fluid particle distributions at neighboring nodes, making all the calculations localized in space. The macroscopic properties of the flow such as density and velocity at each time step can be determined by solving for the fluid particle distributions throughout the grid.

The LBM has been well documented and shown to converge to solve the Navier–Stokes equations for fluid flow.[2] Due to the inherently local nature of calculations used, the LBM is optimal for parallelization on cluster computational resources. This makes the LBM an efficient, accurate, and cost-effective method for solving complex fluid flow problems.

A detailed explanation of the LBM can be found in the recent review article by Aidun and Clausen.[1]

Fluid–Solid Interaction

The solid particles in the suspension use Lagrangian reference frames that move continuously through the fixed Eulerian fluid domain. The solid particle surface is mapped on the Lagrangian frame by boundary nodes, creating a mesh of surface elements. Instead of the traditional bounce-back method for fluid–solid coupling, a novel EBF method is used. In the EBF method, the moving Lagrangian frame for the solid particle allows for the exact position of the solid boundary surface nodes to be determined within the fixed fluid domain. The traditional bounce-back method of solving the solid phase assumes that the solid boundary surface is always located halfway between lattice velocity links, creating a jagged

fluid–solid interaction boundary. The two frames of reference used in the EBF method allow for a smoother and more accurate fluid–solid interaction boundary. The Dirac delta function[21] is used to interpolate the fluid velocities at the solid boundary nodes. The EBF is the fluid–solid interaction force required to impose the no-slip boundary condition at each node in the fluid–solid boundary interface. The EBF is then added directly as an additional force term to the lattice-Boltzmann equation for solving fluid flow. For the solid phase, the motion and orientation of the particles are obtained by solving the Newtonian dynamics equations for the EBF. The EBF method has been validated as second-order accurate and has been described in detail by Wu and Aidun.[26,27]

The LBM-EBF method provides a significant advantage over other suspension flow modelers by using separate resolution scales for the fluid and solid phases. This allows for the modeling of very small particles such as platelets without the need for a fluid grid with the same resolution. This multiscaling ability significantly lowers computational cost while still providing highly accurate results. Figures 3 and 4 demonstrate the different domain types used for the fluid and solid phases in the LBM-EBF method. In addition, the LBM-EBF method models real particles with a surface and volume, allowing for the accurate calculation of shear stress on a particle surface. This ability to calculate shear stress accurately is important in determining platelet activation caused by the shear stresses. The ability of the LBM-EBF method to model real particles is a significant advantage over previous computational studies of platelet activation which have assumed the platelets to be point particles with no surface or volume. This more accurate modeling of the platelet particles in the LBM-EBF method allows for a higher accuracy calculation of blood damage. Thus, the parallel computing, multiscaling, and real particle modeling abilities of the LBM-EBF method make it optimal for the simulations of blood damage and platelet activation.

The full derivation of the LBM-EBF method and validation cases are presented in the Appendix. In addition, the LBM-EBF method has been reviewed by Aidun and Clausen.[1]

RESULTS

Experimental Results of Channel Flows

The TAT concentrations for all eight experimental channels after 60 min are shown in Fig. 5. The plot shows that all of the channels with small minimum diameter of 400 μm (odd-numbered channels) have approximately the same level of TAT concentration. However, the channels with a larger minimum diameter of 800 μm (even-numbered channels) show significant differences in TAT concentration between the geometries. Figure 5 shows that Channel 4 has a significantly higher TAT concentration than Channel 2. These channels have similar geometries except that Channel 2 has a smoother transition to the smaller internal diameter, whereas Channel 4 has a 90-degree angle leading into the smaller internal diameter. Similarly, Channel 8 has a significantly higher TAT concentration than Channel 6. Both of these channels have a larger internal diameter, but Channel 6 has a smoother transition compared to Channel 8, which has a 90-degree angle transition. In addition, Channel 4 has significantly higher TAT concentration than Channel 6, and Channel 8 has significantly higher TAT concentration than Channel 2.

In the numerical simulations, we used the same setup and flow conditions to compare the computational results with the experimental results. TAT concentration results were used as the experimental comparison due to their relative significance compared to the other assays in determining blood damage in the flows through various channels. The hemolysis assay was not sensitive enough and there was no significant difference in plasma hemoglobin concentration for the channels nor was the hemolysis significantly higher than the clinical baseline level for any of the channels. The PF4 assay was too sensitive, as even flow

through a bypass pump would cause the release of PF4. There was not a significant difference in PF4 concentration for the channels at any of the sample times. Furthermore, the cumulative PF4 concentration is well above the baseline level for all of the channels. Thus, all of the channels activate the platelets at about the same level with PF4 concentrations that are at least an order of magnitude higher than the baseline level (20 ng/mL). The TAT concentration results were the most consistent and were sensitive enough to show variation among channels, and were therefore the optimal choice for comparison with the numerical simulations.

Numerical Simulation Results

Figures 6, 7, and 8 show the BDI_G, BDI_T, and BDI_D values for all eight channels, respectively. The platelet surface shear stress is divided by the threshold shear stress τ_{thres} = 105 dyne/cm^2 thres as defined by Tambasco and Steinman,[22] and the exposure time is divided by 1 s, so the BDI values plotted are non-dimensional parameters. These plots show that the profiles of BDI_T and BDI_G are very different in comparison to the experiments. In both models, the non-dimensional BDI values for channels with larger internal diameter (even-numbered channels) are much smaller compared to channels that have the same geometry but smaller internal diameter (odd-numbered channels). However, the results of the BDI_D model are very similar to the experimental results as shown in Fig. 8, except for Channels 4 and 8. One possible reason for this deviation is that in contrast to experiments, in the simulations no platelets enter the recirculation zone at the sharp corners of the channel. Due to the lack of experimental disturbances and flow fluctuations in the computational simulations, fluid or suspended particles cannot cross the streamline surrounding the recirculation zone. Naturally, all 40 platelets that were released at the inlet in the simulation went through the channel without entering the recirculation zone. However, in Fallon *et al.*'s experiments,[6,7] platelets that enter the recirculation zone remain there for a longer period of time compared to other platelets traveling directly through the channel. Since the shear stress in the recirculation zone is high, the BDI value of platelets inside the recirculation zone will strongly affect the average BDI value of the channel. This difference between experiment and simulation becomes significant for Channels 4 and 8, both having sharp transition corners with larger internal diameter and recirculation zones.

In Fig. 8, the BDI_D value of Channel 4 is higher than Channel 2. These two channels have the same dimensions except that Channel 4 has a sharp 90-degree angle leading into the smaller internal diameter and Channel 2 has a much smoother transition to converge to the internal diameter. The sharper angle leads to higher shear stresses, hence the larger damage in Channel 4. Channels 8 and 6 have a similar situation except their geometry is diverging instead of converging.

All four channels with smaller internal diameter (odd-numbered channels) have similar BDI values compared with each other. They also have significantly larger BDI values than the channels with larger internal diameter (even-numbered channels). Based on these simulation results, it is evident that for the small channels, size is more important to blood damage than geometry. For the channels with larger diameter, the geometry does play an important role. It was also found that large recirculation zones or sudden shape transitions will increase platelet activation.

The secondary approach for computing BDI values is applied to all eight channels for the BDI_D model only, as the other two BDI models match very poorly with the experimental results. The time evolution of the BDI_{D_t} values for all channels is plotted in Fig. 9, where the BDI_{D_t} values increase almost linearly. Since the jet velocity at the center of the channel is very high (maximum velocity is 14 m/s and the channel length is 1.5 mm), the platelet at the center of the channel is going through the channel ten times in 1 ms. Figure 10 shows the

BDI_{D_t} values at time equal to 12.5 ms and the pattern is similar to Fallon *et al*.'s experimental results.[6,7]

DISCUSSION

One aim of this study is to match the results of the numerical simulations of platelet flow through different channel geometries with the experimental results of Fallon. In this section, the results and limitations of the BDI_G (Giersiepen *et al*.[10]), BDI_D (Dumont *et al*.[5]), and BDI_T (Tambasco and Steinman[22]) models will be discussed. The numerical procedure that is most appropriate for calculating the BDI value of platelet flow will also be chosen. The selection of an appropriate BDI model that matches the numerical results with the experimental results will allow for future computational studies of determining BDI values in platelet flow through the hinge area of BMHVs.

BDI Models

In our simulations, the BDI_G of a platelet which experiences a shear stress of 200 dynes/cm^2 is approximately 8,000 times larger than the BDI_G for a platelet that experiences a shear stress of 10 dynes/cm^2. This non-linear relation from the BDI_G model causes the significant differences between the BDI values of small channels (odd-numbered channels) and large channels (even-numbered channels). One reason for this large difference is that the exponent constant in this model is based on experiments that have very different flow conditions. In Wurzinger *et al*.'s experiments,[28-30] platelet activation was investigated in a viscometer under constant shear stress. However, in Fallon's experiments and in our simulations, the shear stresses vary significantly from the wall to the center of the channel. This flow condition difference can change the value of the exponent constant in the BDI_G model.

In the present simulation, the BDI_D model gives the closest BDI value pattern when compared to the experimental results as shown in Fig. 8. The limitation of the BDI_D model, as pointed out by Tambasco and Steinman,[22] is that a platelet should only be activated when the platelet shear stress is higher than a threshold value. In the BDI_T model given by Eq. (2), this value is defined as the threshold shear stress and is set at 105 dynes/cm^2. The physical definition of the threshold shear stress is that if the platelet surface shear stress is lower than this value, the platelet should not be activated and the exposure time is irrelevant. The same threshold shear stress value is used in the current model. Based on the simulation results as shown in Fig. 7, this threshold value is too high and most shear stresses on the platelets in large channels (even-numbered channels) were filtered out. Early experiments[4,24,25] have shown platelet secretion and aggregation when the shear stress was higher than 50 dynes/cm^2. Recent studies[12,13,18,19] have demonstrated that at a high level of shear stress (>100 dynes/cm^2), platelets have aggregation and shedding of microparticles from their membrane. Platelets that experience a sustained duration shear stress as low as 12 dynes/cm^2 can also be activated, though only if the exposure time is sufficiently long. The appropriate threshold shear stress should lie between 12 dynes/cm^2 (the physiological shear stress) and 105 dynes/cm^2 (at which significant platelet activation is observed).

Numerical Procedure for BDI

An objective of this research is to choose an appropriate BDI model to optimize the design of BMHVs. All current BDI models are Lagrangian-based models for platelets, and most of these models require the damage accumulation model to estimate the damage caused by the platelet shear stress–time history. This is accurate for estimating the activation state of each platelet. However, this can cause problems when evaluating the design of a channel or BMHV. The initial conditions, such as the initial position, orientation, and release time of the platelets, will affect the BDI value of the channel. For example, Fig. 11 shows a path line

in a pressure-driven channel flow. The BDI values from any existing BDI model will be different for platelets that are released at points *A*, *B*, *C*, and *D*. Moreover, for the BDI models with damage accumulation, the shear stress distribution from points *C* to *D* is always more important than the distribution from points *A* to *B*. In other words, the downstream shear stress distribution will always be more important than the upstream distribution in these BDI models. The BDI value of a channel should only depend on the channel geometry and flow conditions, such as pressure gradient, and should not depend on the initial conditions of the released particles.

The presence of the recirculation zone makes the situation even more complex. If the platelets are only released at the inlet, these particles will not enter the recirculation zone (assuming no recirculation zone exists at the inlet of the fluid domain). The shear stress in the recirculation zone is high, and the platelets trapped in the zone experience a longer exposure time. Thus, the recirculation zone is an important part of the blood damage and is very important for BDI calculation.

One solution to address these problems is to calculate the space-averaged shear stress within the channel. However, the blood damage should depend not only on the local shear stress like in this solution, but also on the number of platelets that pass through a given region. Thus, this option is unrealistic and we propose a secondary approach: the addition of a random disturbance force to include the recirculation zones in the platelet flow. The damage accumulation model is removed so that the BDI value depends only on the channel geometry and flow conditions. Because platelets are pushed toward the wall in blood flow, the BDI value of every platelet is weighted by the local platelet concentration at the inlet position. In the secondary method, the BDI value of a channel with a fixed pressure gradient should increase over time as shown in Fig. 9. The channel that has a higher pressure gradient should have a higher BDI value compared to a channel that has the same geometry but a lower pressure gradient.

Compared to the results from the old method as shown in Fig. 8, this new method greatly improves the BDI value estimation in the recirculation zone. As shown in Figs. 10 and 8, the patterns of the results for small channels (odd-numbered channels) are similar. The BDI values for the small channels in both the old and new methods have similar values. However, the patterns for the large channels (even-numbered channels) using these two methods are very different. In the new method, the channels with sharp transition area have much higher BDI values compared to the channels with smooth transition area. This difference in BDI values in the large channels is not significant in the old method as shown in Fig. 8. The reason for the change in results is that in the new method, platelets can enter the recirculation zone. This new numerical procedure can be used to assess the blood damage in BMHV hinges under different flow conditions (pressure gradient, unsteady flow, etc.).

In Fig. 10, we see that for the small channels, the BDI_{D_t} values are relatively similar for each of the geometry types. For the large channels, the BDI_{D_t} values are significantly higher for the channels with sharp transition geometry in comparison to the channels with a smooth transition. We can deduce here that as the constriction diameter decreases, the geometry of the constriction area plays a smaller factor. Typical BMHV hinge gap widths are from 100 to 200 μm but can be larger in neighboring areas, thus making the relative significance of shape geometry unknown for BMHV hinge gaps. Future numerical studies will explore the impact of constriction size and geometry on blood damage in BMHV hinge gaps with various hinge designs.

CONCLUSIONS

In this study we use a novel multiscale method for the direct simulation of platelet flow to determine the effects of channel geometry design on blood damage. Platelets can have different shapes: healthy platelets have an ellipsoidal disk shape, and activated platelets have a rounded shape with irregular tassels. Thus, the unsteady shear stress sensed by platelets is not the same as for a spherical particle. It is imperative to develop a particle-level numerical method with two-way coupling between the fluid and solid phases.

The BDI values computed for different channels are compared to previously published experimental data.[6,7] Comparison of our simulations with experimental results shows a similar pattern of BDI values and shows that Dumont's BDI model[5] is the most appropriate for blood damage investigation. A new numerical procedure is proposed in this study to include the presence of recirculation zones in the BDI calculation and to eliminate the effects of initial conditions. Furthermore, the simulations come to the same conclusion as the experiments[6,7]: that channels with sharp contraction–expansion areas will have larger recirculation zones that cause elevated BDI values. For channels with large internal diameter, geometry is a significant factor in blood damage. For channels with small internal diameter, size plays a more important role in blood damage than channel geometry. We deduce that as constriction diameter decreases, size will play an increasingly significant role in blood damage in comparison to channel geometry.

Acknowledgments

This research was carried out under a grant from the National Heart, Lung and Blood Institute (HL-07262). This research was partially funded by Tom and Shirley Gurley.

Appendix

APPENDIX:

Experimental Assay Methods

TAT ELISA

The presence of TAT in the samples was measured using an Enzygnost TAT microassay (Dade Behring, Deerfield, IL, USA). Absorbance was determined using a SpectraMax Plus 384 microplate reader (Molecular Devices, Sunnyvale, CA, USA) at a wavelength of 492 nm. Samples exceeding the highest standard were diluted and re-assayed.

PF4 ELISA

PF4 was measured using a Zymutest PF4 microassay (Hyphen Biomed, Neuville sur Oise, France). Absorbance was determined using a SpectraMax Plus 384 (Molecular Devices) at a wavelength of 450 nm. The standard curve ranged from 0.5 to 10 g/L. Samples with higher concentrations were diluted with sample diluent prior to the start of the assay.

Hemolysis Assay

Hemolysis in the samples was determined using a microplate assay. The plasma samples were mixed with Drabkins reagent in a 1:9 ratio of plasma to Drabkins reagent, and 200 mL of the mixture was added to each of the wells. The resulting color intensities of the samples were measured with a microtiter absorbance plate reader (SpectraMax Plus 384, Molecular Devices) at a wavelength of 540 nm. A standard curve was constructed with known amounts of whole blood and Drabkins reagent, and from the standard curve the concentration of hemoglobin in each of the samples was determined. The standards were prepared by

measuring the RBC count and hemoglobin concentration of the whole blood using a cell counter (Coulter MAX). This whole blood was then mixed with different amounts of Drabkins reagent to obtain a range of hemoglobin concentrations from 0 to 5.48 mg/mL.

EBF Method for Fluid–Solid Interaction

The EBF is the fluid–solid interaction force used to impose the no-slip boundary condition at the platelet surface. Let Π_s and Π_f represent the continuum solid and fluid domains, Γ the fluid–solid boundary, and Γ_s and Γ_f be subsets for the solid and fluid boundary nodes. $\boldsymbol{F}^{\text{fsi}}(\boldsymbol{x}, t)$ and $\boldsymbol{g}(\boldsymbol{x}, t)$ represent the force density (force per unit volume) acting, respectively, on the solid and the fluid at the boundary nodes $\boldsymbol{x}$ on Γ at time t. Therefore, by Newton's third law, $\boldsymbol{F}^{\text{fsi}}(\boldsymbol{x}, t) = -\boldsymbol{g}(\boldsymbol{x}, t)$ for $\boldsymbol{x} \in \Gamma$. The motion of the fluid is governed by the Navier–Stokes and continuity equations with the inclusion of the EBF, which can be written as

$$\left.\begin{array}{l} \rho\left(\frac{\partial \boldsymbol{u}}{\partial t} + \boldsymbol{u}\cdot\nabla\boldsymbol{u}\right) = -\nabla P + \mu\nabla^2\boldsymbol{u} + \boldsymbol{g}(\boldsymbol{x}, t) \\ \nabla\cdot\boldsymbol{u} = 0 \end{array}\right\}, \tag{4}$$

where $\boldsymbol{x} \in \Pi_f$. In the first equation, $\boldsymbol{g}(\boldsymbol{x}, t) = 0$ when $\boldsymbol{x} \notin \Gamma$. In the discretized formulation, the EBF $\boldsymbol{g}$ is evaluated on the fluid boundary node as shown in Eq. (7).

To calculate the fluid–solid interaction force, we first calculate the fluid velocity $\boldsymbol{U}_f\left(\boldsymbol{x}_j^i, t\right)$ at solid boundary node $\boldsymbol{x}_j^i$ at time t,

$$\boldsymbol{U}_f\left(\boldsymbol{x}_j^i, t\right) = \int_{\Pi_f} \boldsymbol{u}(\boldsymbol{x}^e, t)\, D\left(\boldsymbol{x}^e - \boldsymbol{x}_j^i\right) d\boldsymbol{x}^e, \quad \boldsymbol{x}_j^i \in \Gamma_s, \tag{5}$$

where $\boldsymbol{x}_j^i$ is the position vector for the jth solid node on the ith platelet, $\boldsymbol{x}^e$ represents the position for the vector fluid nodes, and $D\left(\boldsymbol{x}^e - \boldsymbol{x}_j^i\right)$ is the Dirac delta function.[21]

Assuming that the platelet will move with the velocity at the previous time step, the fluid–solid interaction force $\boldsymbol{F}^{\text{fsi}}\left(\boldsymbol{x}_j^i, t\right)$ at the platelet boundary node is given by

$$\begin{array}{l} \boldsymbol{F}^{\text{fsi}}\left(\boldsymbol{x}_j^i, t\right) = \rho_f\left(\boldsymbol{U}_f\left(\boldsymbol{x}_j^i, t\right) - \boldsymbol{U}_p\left(\boldsymbol{x}_j^i, t - \Delta t^{\text{LBM}}\right)\right)/\Delta t^{\text{LBM}}, \\ \boldsymbol{x}_j^i \in \Gamma_s, \end{array} \tag{6}$$

where ρ_f is the density of the fluid and $\Delta t^{\text{LBM}} = 1$ is the LBM time step. The resulting force acting on the fluid is given by

$$\boldsymbol{g}(\boldsymbol{x}^e, t) = -\int_\Gamma \boldsymbol{F}^{\text{fsi}}\left(\boldsymbol{x}_j^i, t\right) D\left(\boldsymbol{x}^e - \boldsymbol{x}_j^i\right) d\boldsymbol{x}_j^i, \quad \boldsymbol{x}^e \in \Gamma_f, \tag{7}$$

where $\boldsymbol{g}$ will be used as an EBF term in the lattice-Boltzmann equation as discussed in the following section.

Once the total force and torque are obtained for each platelet, the velocity and angular velocity of the suspending platelets can be computed by the numerical solution of the Newtonian dynamics equations.

Lattice-Boltzmann with External Boundary Force

The state of the fluid at node $\boldsymbol{x}^{\mathrm{e}}$ at time t is described by the distribution function $f_k(\boldsymbol{x}^{\mathrm{e}}, t)$, which is calculated through the lattice-Boltzmann equation[2,14,17]

$$f_k\left(\boldsymbol{x}^{\mathrm{e}}+\boldsymbol{e}_k, t+\Delta t^{\mathrm{LBM}}\right) = f_k(\boldsymbol{x}^{e}, t)+\frac{1}{\lambda}\left[f_k^{\mathrm{eq}}(\boldsymbol{x}^{\mathrm{e}}, t)-f_k(\boldsymbol{x}^{\mathrm{e}}, t)\right]. \tag{8}$$

Here, $f_k^{\mathrm{eq}}(\boldsymbol{x}^{\mathrm{e}}, t)$ is the equilibrium distribution function at $\boldsymbol{x}^{\mathrm{e}}$ at time t, λ the single relaxation time constant, and $\boldsymbol{e}_k$ the discrete velocity vector. The fluid density ρ_{f} and the macroscopic fluid velocity $\boldsymbol{u}(\boldsymbol{x}^{\mathrm{e}}, t)$ are obtained from the first two moments of the distribution function, given by

$$\rho_{\mathrm{f}}(\boldsymbol{x}^{\mathrm{e}}, t)=\sum_k f_k(\boldsymbol{x}^{\mathrm{e}}, t) \quad \text{and}$$
$$\rho_{\mathrm{f}}(\boldsymbol{x}^{\mathrm{e}}, t)\,\boldsymbol{u}(\boldsymbol{x}^{\mathrm{e}}, t)=\sum_k f_k(\boldsymbol{x}^{\mathrm{e}}, t)\cdot\boldsymbol{e}_k. \tag{9}$$

The most common lattice model for 3D simulations is the D3Q19 model, which uses nineteen discrete velocity directions. The equilibrium distribution function is defined as

$$f_k^{\mathrm{eq}}=w_k\rho\left[1+3\boldsymbol{e}_k\cdot\boldsymbol{u}+\frac{9}{2}(\boldsymbol{e}_k\cdot\boldsymbol{u})^2-\frac{3}{2}|\boldsymbol{u}|^2\right], \tag{10}$$

where $w_0 = 1/3$, $w_{1–6} = 1/18$ (non-diagonal directions), and $w_{7–18} = 1/36$ (diagonal directions) in the 3D D3Q19 model. For the present model, the speed of sound is $c_s=\sqrt{1/3}$ and the kinematic viscosity is $v = (2\lambda - 1)/6$.

The fluid–solid interaction force $\boldsymbol{g}$ from Eq. (7) becomes an additional term to the collision function and is included in the lattice-Boltzmann equation as

$$f_k\left(\boldsymbol{x}^{\mathrm{e}}+\boldsymbol{e}_k, t+\Delta t^{\mathrm{LBM}}\right) = f_k(\boldsymbol{x}^{\mathrm{e}}, t)+\frac{1}{\lambda}\left[f_k^{\mathrm{eq}}(\boldsymbol{x}^{\mathrm{e}}, t)-f_k(\boldsymbol{x}^{\mathrm{e}}, t)\right]+\frac{3}{2}w_k\boldsymbol{g}\cdot\boldsymbol{e}_k. \tag{11}$$

LBM-EBF Validation

The following are the validation cases of suspension flow for the LBM-EBF method. Additional validation cases can be found in the methodology paper of Wu and Aidun.[26]

An Ellipsoid in Simple Shear Flow

The motion of a solid ellipsoid in a simple shear flow is analyzed in this section. The boundary of this particle is given by

$$\frac{x^2}{a^2}+\frac{y^2}{b^2}+\frac{z^2}{c^2}=1 \tag{12}$$

When one of the principal axes of the ellipsoid is kept parallel to the vorticity vector, as shown in Fig. 12, the rotation angle, ϕ, and the angular rate of rotation, $\dot{\phi}$, are given by Jeffery[15]

$$\phi=\tan^{-1}\left(\frac{b}{a}\tan\frac{abGt}{a^2+b^2}\right) \tag{13}$$

$$\dot{\phi}=\frac{G}{a^2+b^2}\left(b^2\cos^2\phi+a^2\sin^2\phi\right) \tag{14}$$

where G is the shear rate and t is time. In our simulation, the computational domain is 120 × 120 × 60 lattice nodes. The Reynolds number is $Re = Gd^2/\nu$, where $d = 2a$. For different aspect ratios b/a, the computational results agree very well with Jeffery's analytical solution, as shown in Fig. 13. This demonstrates that the no-slip boundary condition on the ellipsoid surface is well satisfied.

RBC in Capillary Pressure-Driven Flow

It is well known from past experiments that the RBC shape changes into a parachute shape in capillary pressure-driven flow, as shown in Fig. 14, retain their shape through the capillary tube, and recover to its original shape in the post-capillary region. This unique deformation of the RBC is necessary in nature for high fluidity in microvessels and for high efficiency of oxygen diffusion to tissue by increasing the surface area and interaction with the endothelial cells.

Several investigators have used this phenomenon to measure the RBC's deformability. In the recent experimental setup of Tsukada *et al*.[23] they use a set of transparent crystal microchannels and a high-speed video camera to capture high-resolution pictures and achieve quantitative data. Dilute suspensions of RBCs passed through a glass capillary tube with a diameter of 9.3 μm were imaged and analyzed. The velocity and the deformation index DI_P of a RBC depends on the pressure gradient in the channel. In this experiment,[23] DI_P is given by

$$DI_P=\frac{c}{d} \tag{15}$$

where d is the diameter of the deformed RBC in the parachute configuration and c is the length of the RBC along the axial direction as shown in Fig. 14. The simulation results are compared with the experimental results.[23] The Capillary number Ca_P in Fig. 15 is defined as

$$Ca_P=\frac{\mu U_x}{S} \tag{16}$$

where μ is the viscosity of the suspending fluid, U_x the RBC velocity, and S the membrane shear modulus.

The RBC deformation index DI_P is shown in Fig. 15 as a function of Capillary number Ca_P. The simulations agree well with experiments up to $Ca_P \approx 0.35$ where we see a deviation between the results.

REFERENCES

1. Aidun CK, Clausen JR. Lattice-boltzmann method for complex flows. Annu. Rev. Fluid Mech. 2010; 42:439.
2. Aidun CK, Lu Y, Ding E. Direct analysis of particulate suspensions with inertia using the discrete Boltzmann equation. J. Fluid Mech. 1998; 373:287.
3. Bluestein D. Research approaches for studying flow induced thromboem-bolic complications in blood recirculating devices. Expert Rev. Med. Dev. 2004; 1:65–80.
4. Brown CH, et al. Morphological, biochemical and functional changes in human platelets subjected to shear stress. J. Lab. Clin. Med. 1975; 86:462. [PubMed: 1151161]
5. Dumont K, et al. Comparison of the hemodynamic and thrombogenic performance of two Bileaflet mechanical heart valves using a CFD/FSI Model. J. Biomech. Eng. 2007; 129:558–565. [PubMed: 17655477]
6. Fallon, AM. The Development of a Novel in vitro Flow System to Evaluate Platelet Activation and Procoagulant Potential Induced by Bileaflet Mechanical Heart Valve Leakage Jets in School of Chemical and Biomolecular Engineering. Georgia Institute of Technology; Atlanta: 2006.
7. Fallon AM, Dasi LP, Marzec UM, Hanson SR, Yoganathan AP. Procoagulant properties of flow fields in stenotic and expansive orifices. Ann. Biomed. Eng. 2008; 36(1):1. [PubMed: 17985244]
8. Fallon AM, Shah N, Marzec UM, Warnock JN, Yoganathan AP, Hanson SR. Flow and thrombosis at orifices simulating mechanical heart valve leakage regions. J. Biomech. Eng. 2006; 128:30. [PubMed: 16532615]
9. Fallon AM, et al. Thrombin formation in vitro in response to shear-induced activation of platelets. Thromb. Res. 2007; 121(3):397–406. [PubMed: 17532367]
10. Giersiepen M, et al. Estimation of shear stress-related blood damage in heart valve prostheses—in vitro comparison of 25 aortic valves. Int. J. Artif. Organs. 1990; 13(5):300–306. [PubMed: 2365485]
11. Grigioni M, et al. Proposal for a new formulation of the power law mathematical model for blood trauma prediction. Biomech. Model. Mechanobiol. 2005; 4:249. [PubMed: 16283225]
12. Hellums JD. Whitaker lecture: biorheology in thrombosis research. Ann. Biomed. Eng. 1994; 22:445. [PubMed: 7825747]
13. Holme PA, et al. Shear-induced platelet activation and platelet microparticle formation at blood flow conditions as in arteries with a severe stenosis. Arterioscler. Thromb. Vasc. Biol. 1997; 17:646–653. [PubMed: 9108776]
14. Hou S, et al. Simulation of cavity flow by lattice Boltzmann method. J. Comput. Phys. 1995; 118(2):329.
15. Jeffery GB. The motion of ellipsoidal particles immersed in a viscous fluid. Proc. R. Soc. Lond. Ser. A. 1922; 102:161.
16. Kroll MH, et al. Platelets and shear stress. Blood. 1996; 88(5):1525–1541. [PubMed: 8781407]
17. McNamara GR, Zanetti G. Use of the Boltzmann equation to simulate lattice-gas automata. Phys. Rev. Lett. 1988; 61:2332. [PubMed: 10039085]
18. Merino A, et al. Synergistic action of severe wall injury and shear forces on thrombus formation in arterial stenosis: definition of a thrombotic shear rate threshold. J. Am. Coll. Cardiol. 1994; 24:1091. [PubMed: 7930203]
19. Miyazaki Y, et al. High shear stress can initiate both platelet aggregation and shedding of procoagulant containing microparticles. Blood. 1996; 88:3456. [PubMed: 8896411]
20. Nobili M, et al. Platelet activation due to hemodynamic shear stresses: damage accumulation model and comparison to in vitro measurements. ASAIO J. 2008; 54:64–72. [PubMed: 18204318]
21. Peskin CS. The immersed boundary method. Acta Numerica. 2002; 11:479.
22. Tambasco M, Steinman DA. Path-dependent hemodynamics of the stenosed carotid bifurcation. Ann. Biomed. Eng. 2003; 31:1054–1065. [PubMed: 14582608]
23. Tsukada K, Sekizuka E, Oshio C. Direct measurement of erythrocyte deformability in diabetes mellitus with transparent microchannel capillary model and high-speed video camera system. Microvasc. Res. 2001; 61:231. [PubMed: 11336534]

24. Weiss HJ, Turitto VT, Baumgartner HR. Effect of shear rate on platelet interaction with subendothelium in citrated and native blood. Shear rate-dependent decrease of adhesion in von Willebrand disease and the Bernard Soulier syndrome. J. Lab. Clin. Med. 1978; 92:750. [PubMed: 309498]

25. Weiss HJ, et al. Correction by factor VIII of the impaired platelet adhesion to subendothelium in von Willebrand's disease. Blood. 1978; 51:267. [PubMed: 304366]

26. Wu J, Aidun CK. Simulating 3D deformable particle suspensions using lattice Boltzmann method with discrete external boundary force. Int. J. Numer. Method Fluids. 2010; 62(7):765–783.

27. Wu J, Aidun CK. A method for direct simulation of flexible fiber suspensions using lattice-Boltzmann equation with external boundary force. Int. J. Multiphase Flow. 2010; 36:202–209.

28. Wurzinger LJ, Opitz R, Eckstein H. Mechanical blood trauma: an overview. Angeiologie. 1986; 38:81–97.

29. Wurzinger LJ, et al. Platelet and coagulation parameters following millisecond exposure to laminar shear stress. Thromb. Haemost. 1985; 54(2):381–386. [PubMed: 2934855]

30. Wurzinger LJ, et al. Ultrastructural investigations on the question of mechanical activation of blood platelets. Ann. Hematol. 1987; 54(2):97–107.

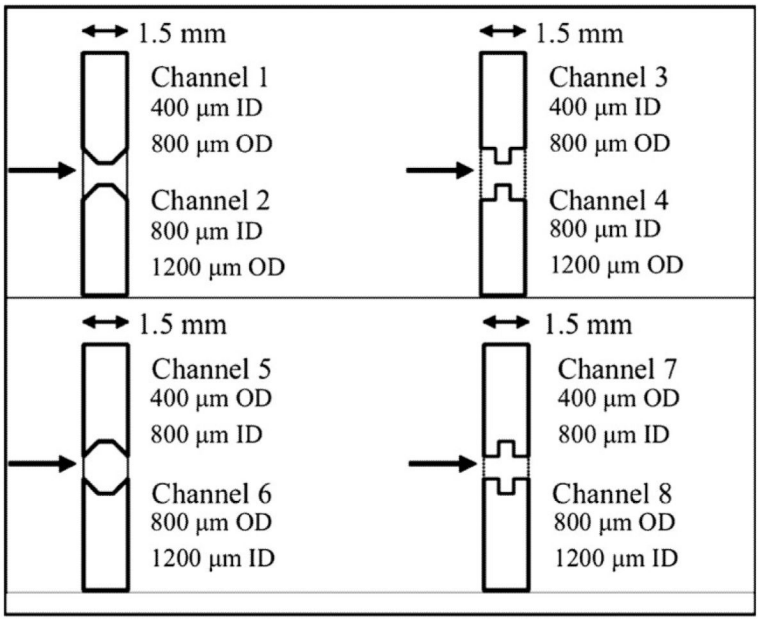

FIGURE 1.

Diagram of channels used in experimental setup and numerical simulations (from Fallon *et al*.[6,7]). Odd-numbered channels have smaller diameters compared to even-numbered channels of similar geometry.

FIGURE 2.

Flowchart as an overview of the LBM-EBF method. Fluid phase is solved by the LBM, solid phase is solved by Newtonian dynamics, and the fluid–solid interaction is computed by the EBF method.

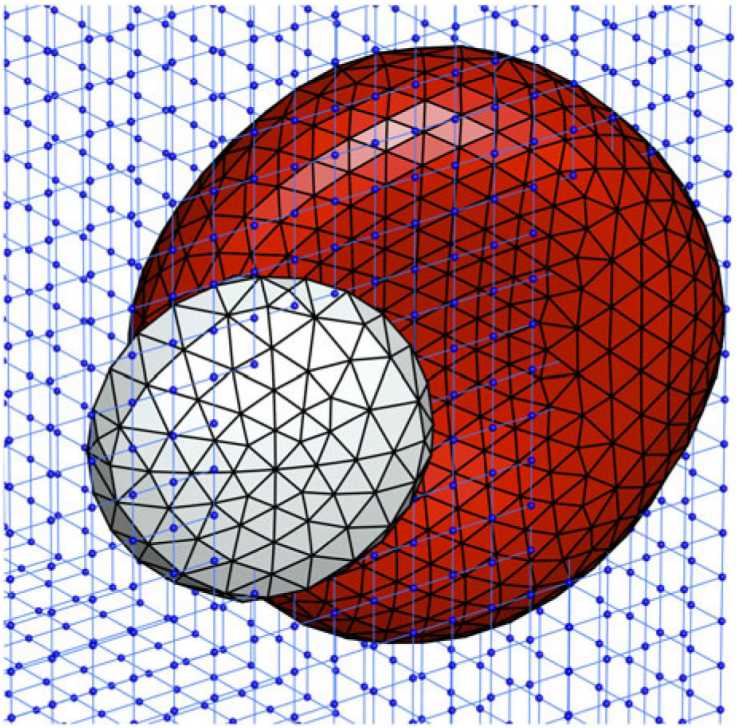

FIGURE 3.
Diagram demonstrating the multiscaling ability of LBM-EBF. Includes one model red blood cell and white platelet with separate solid meshes within a fixed lattice-Boltzmann 3D fluid grid.

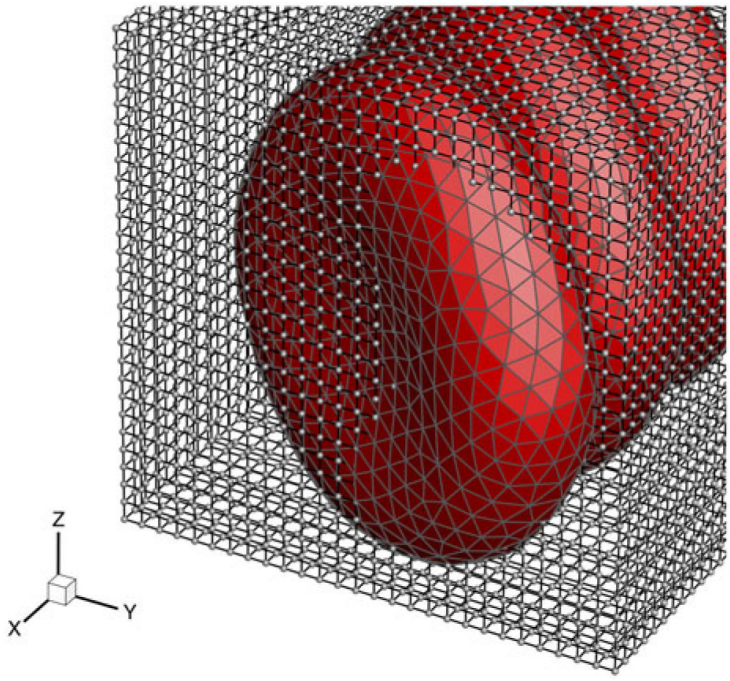

FIGURE 4.

Diagram demonstrating the multiscaling ability of LBM-EBF. Includes three model red blood cells within a lattice-Boltzmann 3D fluid grid. One can clearly discern the difference between the fixed fluid grid and the solid particle mesh.

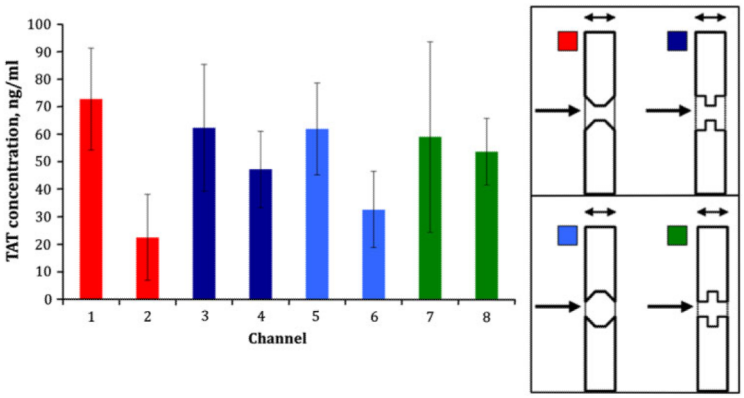

FIGURE 5.

Fallon's experimental results of TAT concentration for all of the channels the channels at 60 min (from Fallon *et al*.[6,7]). The odd-numbered smaller diameter channels have higher TAT concentration than the larger diameter even-numbered channels. Also, sharper contraction/ expansion geometries result in higher TAT concentration.

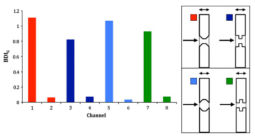

FIGURE 6.

BDI_G for all eight channels, LBM-EBF simulation results. This BDI model agrees poorly with the experimental data, particularly for the larger diameter even-numbered channels.

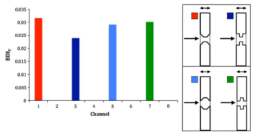

FIGURE 7.

BDI_T for all eight channels, LBM-EBF simulation results. This BDI model agrees very poorly with the experimental results. The even-numbered channels' BDI values are much smaller than the odd-numbered channels' BDI values due to the threshold shear stress value for BDI_T.

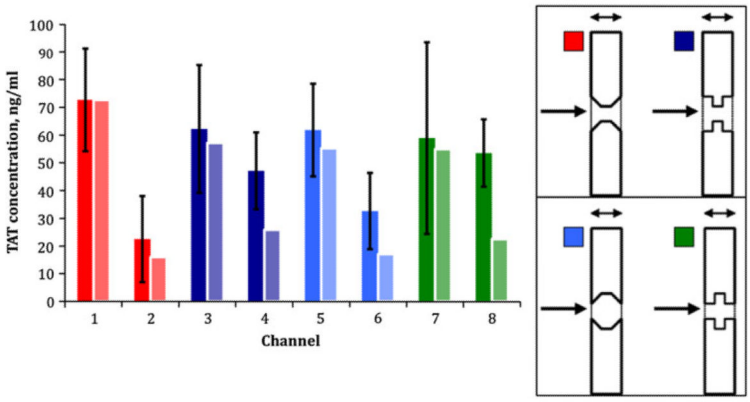

FIGURE 8.

BDI_D model comparison for all eight channels. The lighter shade right-side bars are the LBM-EBF simulation results for BDI_D and the darker shade left-side bars are the TAT concentrations from Fallon's experiment as shown in Fig. 5. The numerical and experimental results are matched for Channel 1 as a reference point. The results agree well for the remaining channels except for Channels 4 and 8.

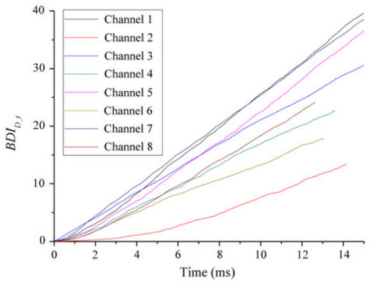

FIGURE 9.
Time evolution of BDI_{D_t} for all eight channels. BDI values increase over time in a pressure-driven flow as expected.

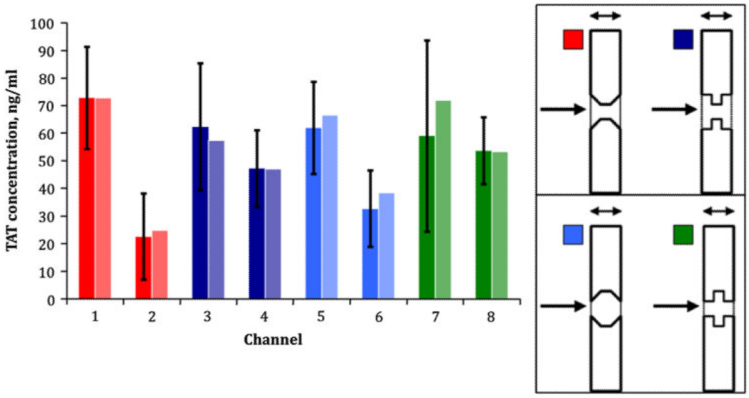

FIGURE 10.

BDI_{D_t} model comparison for all eight channels at time equal to 12.5 ms. The lighter shade right-side bars are the LBM-EBF simulation results for BDI_{D_t} and the darker shade left-side bars are the TAT concentrations from Fallon's experiment as shown in Fig. 5. The numerical and experimental results are matched for Channel 1 as a reference point. The numerical and experimental results agree well for the remaining channels.

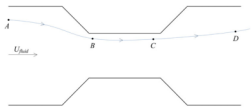

FIGURE 11.

A path line in a pressure-driven channel flow. Although BDI values should depend on flow conditions and channel geometry only, this diagram shows that the initial position of platelets is an important factor in the current damage accumulation BDI models.

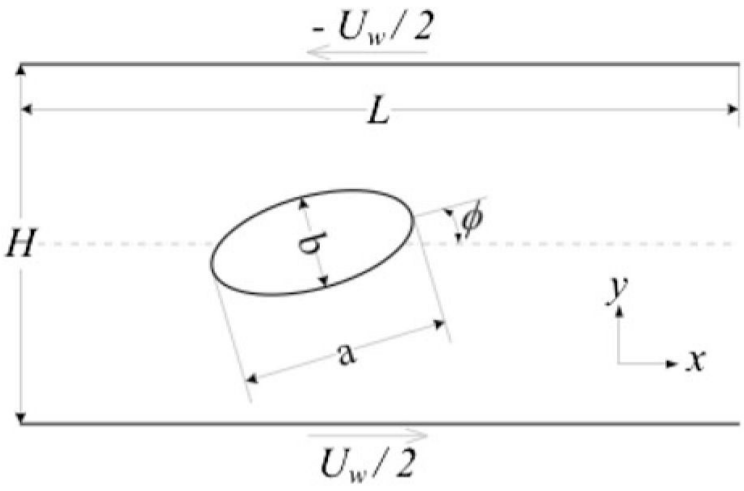

FIGURE 12.
A solid ellipsoid immersed in simple shear flow, known as Jeffery's orbit.

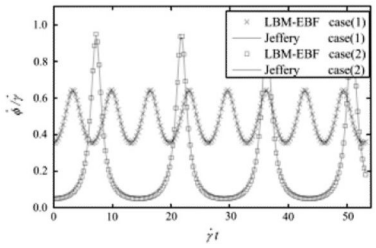

FIGURE 13.

$G = 1/600$, $a = 12$, $v = 1.5$, $Re = 0.064$. Case(1): $b = c = 9$, the solid line is Jeffery's solution[15] and the crosses (×) are the simulation results. Case(2): $b = c = 3$, the dash line is Jeffery's solution and the open squares are the simulation results. The LBM-EBF simulation results agree very well with Jeffery's solution.

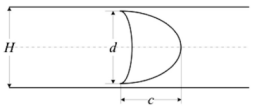

FIGURE 14.
Axisymmetrically deformed RBC in a ‘parachute configuration’ in capillary pressure-driven flow.

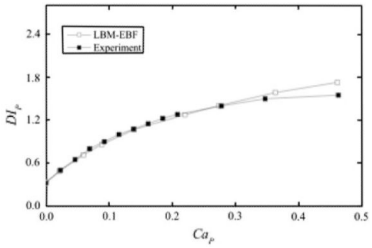

FIGURE 15.

Deformation index DI_P vs. capillary number Ca_P. The solid squares are the experimental data from Tsukada *et al.*[23] and the open squares are the LBM-EBF simulation results. The numerical and experimental results agree very well up to $Ca_P \approx 0.35$.